A climosequence of chronosequences in southwestern Australia

Benjamin L. Turner[1,2*], Patrick E. Hayes[2], Etienne Laliberté[3,2]

[1]Smithsonian Tropical Research Institute, Apartado 0843-03092, Balboa, Ancon, Republic of Panama

[2]School of Biological Sciences, The University of Western Australia, 35 Stirling Highway, Crawley, Perth, WA 6009, Australia

[3]Centre sur la biodiversité, Institut de recherche en biologie végétale, Département de sciences biologiques, Université de Montréal, 4101 Sherbrooke Est, Montréal H1X 2B2, Canada

*Corresponding author: TurnerBL@si.edu

Abstract

To examine how climate affects soil development and nutrient availability over long timescales, we studied a series of four long-term chronosequences along a climate gradient in southwestern Australia. Annual rainfall ranged from 533 mm to 1185 mm (water balance from –900 mm to +52 mm) and each chronosequence included Holocene (≤6.5 ka), Middle Pleistocene (120–500 ka), and Early Pleistocene (~2000 ka) dunes. Vegetation changed markedly along the climosequence, from shrubland at the driest site to *Eucalyptus* forest at the wettest. The carbonate and P content of the parent sand declined along the climosequence, presumably linked to variation in offshore productivity. However, soil development and associated nutrient status followed remarkably consistent patterns along the four chronosequences. Pedogenesis involved decalcification and secondary carbonate precipitation in Holocene soils and leaching of iron oxides from Middle Pleistocene soils, ultimately yielding bleached quartz sands on the oldest soils. Along all chronosequences soil pH and total P declined, while C:P and N:P ratios increased, consistent with the predicted shift from N to P limitation of vegetation during ecosystem development. The expected unimodal pattern of leaf area index was most pronounced along wetter chronosequences, suggesting an influence of climate on the expression of retrogression. The four chronosequences do not appear to span a pedogenic climate threshold, because exchangeable phosphate and base cations declined consistently during long-term pedogenesis. However, the proportion of the total P in organic form was greater along wetter chronosequences. We conclude that soils and nutrient availability on the coastal sand plains of southwestern Australia change consistently during long-term pedogenesis, despite marked variation in modern vegetation and climate. The four chronosequences provide a rare soil-age × climate framework within which to study long-term ecosystem development.

Introduction

Pedogenesis over thousands to millions of years involves marked changes in nutrient availability (Vitousek, 2004). In particular, nitrogen (N) increases in the early stages of ecosystem development through biological N fixation, whereas phosphorus (P) availability declines continuously as P is lost by leaching at a greater rate than it is replenished by weathering or atmospheric inputs (Walker & Syers, 1976). This drives a long-term shift from N to P limitation of plant biomass and productivity (Vitousek & Farrington, 1997; Wardle *et al.*, 2004; Laliberté *et al.*, 2012), which is reflected in marked changes in the diversity and function of plant and microbial communities (Williamson *et al.*, 2005; Jangid *et al.*, 2013; Laliberté *et al.*, 2013; Zemunik *et al.*, 2015).

Rates of pedogenesis and nutrient depletion influenced markedly by climate (Chadwick & Chorover, 2001; Selmants & Hart, 2010; Feng *et al.*, 2016). Assuming other soil-forming factors are held constant (i.e. topography, parent material, and vegetation), wetter sites are expected to lose rock-derived nutrients at a greater rate than comparable drier sites due to accelerated weathering and greater leaching losses. However, vegetation typically co-varies with climate and might mitigate nutrient loss. For example, wetter sites tend to support greater plant biomass than drier sites, retaining nutrients in the system and reducing the rate of nutrient loss by leaching, at least when precipitation is in balance with potential evapotranspiration (Porder & Chadwick, 2009). In contrast, arid ecosystems lose nutrients more slowly through reduced leaching but support little plant biomass, and therefore have a limited potential to retain nutrients over long timescales. In other words, plants might be able to influence the rate of nutrient loss during pedogenesis depending on the extent to which they retain nutrients in the plant-soil system, which itself depends on climate (Porder & Chadwick, 2009).

Despite the significance of this soil development model to our understanding of terrestrial nutrient cycling, it has been tested only once (Porder & Chadwick, 2009). This is because doing so requires multiple long-term soil chronosequences that are similar to terms of parent material, topography, and time, yet that differ in terms of potential evapotranspiration, precipitation, and water balance. Model systems that meet these strict requirements are exceedingly rare – so far only the well-studied Hawaiian Island sequence has been suitable. Porder and Chadwick (2009) studied three basalt lava flows on Hawaii varying from 10,000 to 350,000 years old, with annual precipitation ranging from 500 to 2500 mm. At relatively dry sites (< 750 mm annual rainfall) where evapotranspiration exceeded precipitation, plants slowed nutrient loss, but the effect was small since there was little plant biomass. At intermediate rainfall sites (750–1400 mm) where potential evapotranspiration exceeded precipitation (i.e., negative water balance), plants uplift of nutrients enriched the soil surface with P for at least 350,000 years, effectively compensating for leaching losses. In contrast, at the wettest sites (>1500 mm annual rainfall) where precipitation exceeded evapotranspiration (i.e., positive water balance), leaching losses overwhelmed the capacity of plants to retain nutrients after 350,000 years of pedogenesis, despite greater biomass. Indeed, on much older soils (Oxisols approximately 4 million years old) this 'high rainfall' process domain (see below) occurred above about 900 mm of annual rainfall (compared to 1500 mm on younger soils), presumably reflecting long-term depletion of P, reduced productivity, and therefore a reduced capacity of the ecosystem to retain nutrients against leaching losses (Vitousek & Chadwick, 2013a). The influence of plants on nutrient retention therefore appears to be strongest where potential

evapotranspiration is roughly in balance with precipitation, although this can be overridden on strongly weathered soils when extreme P limitation reduces the capacity of plants to retain nutrients in the ecosystem.

The rainfall zones described by Porder and Chadwick (2009) for P dynamics reflect the balance between precipitation and evapotranspiration, and correspond to 'soil process domains' (Vitousek & Chadwick, 2013a), defined as climate zones within which soils appear to change relatively little across broad variation in rainfall. The domains are separated by pedogenic thresholds, where soil properties vary abruptly across a relatively short variation in rainfall (Chadwick & Chorover, 2001). For basaltic soils on Hawaii subject to about 150,000 years of pedogenesis, the process domains correspond to soils where evapotranspiration exceeds precipitation and carbonate accumulation dominates pedogenesis (low rainfall < 700 mm), a domain where evapotranspiration is slightly greater than precipitation (700 to 1500 mm) and plant uplift and retention of nutrients can compensate for leaching losses, a wetter domain (1500 to 2500 mm) where precipitation exceeds evapotranspiration and pedogenesis is dominated by the accumulation of metal oxides (Chadwick *et al.*, 2003), and a very wet domain (> 2500 mm) where saturation causes iron to be solubilised and lost via reduction and leaching (Chadwick & Chorover, 2001; Vitousek & Chadwick, 2013a). Above the threshold where precipitation exceeds evapotranspiration the soils exhibit a decline in pH, a decline in base cations and base saturation, and an increase in exchangeable Al (Chadwick *et al.*, 2003). These changes are linked to the depletion of primary minerals and leaching at a greater rate than replenished by weathering.

Here we report a study of a series of four long-term (Early Pleistocene) chronosequences along a rainfall gradient in southwestern Australia. Our recent study of soil development along the Jurien Bay chronosequence in Western Australia, corresponding to the driest chronosequence in the present study, shows a characteristic pattern of soil development, with decalcification of young carbonate-rich dunes, formation of a petrocalcic horizon, and leaching of iron oxide coatings on sand grains leaving bleached quartz sands many meters deep (Turner & Laliberté, 2015). These changes correspond with marked depletion of soil P and other nutrients, leading to some of the most infertile soils in the world on the oldest dunes. Here we extend our Jurien Bay work to similar coastal dune deposits extending hundreds of kilometers south along a strong climate gradient, allowing us to identify three additional long-term soil chronosequences with similar aged dunes but contrasting water balance. Our aim was to use this climosequence of chronosequences along the coast of southwestern Australia to examine how climate influences soil development and nutrient availability during long-term pedogenesis.

Materials and Methods

Regional overview and description of the chronosequences

A series of dune deposits occur along parallel to the coast of southwestern Australia, running for approximately 400 km from Geraldton in the north to Dunsborough in the south (Fig. 1). Known as the Swan Coastal Plain, the dunes were formed by periodic interglacial sea-level high stands since the Early Pleistocene or Late Pliocene (*i.e.* 2.59 million years ago) (Kendrick *et al.*, 1991). An additional area of dunes along the southern coastline near Pemberton and Northcliffe, the Scott

Coastal Plain, is assumed to correspond to the main dune deposits on the Swan Coastal Plain (Playford *et al.*, 1976). The dunes and their associated soils are grouped into three main units according to the underlying parent sand deposits (McArthur & Bettenay, 1974; Playford *et al.*, 1976). The Quindalup dunes of Holocene age (up to 6500 years old) and correspond with the Safety Bay Sand, the Spearwood dunes are of Middle Pleistocene age (120,000 to 500,000 years old) and correspond with the Tamala Limestone, and the Bassendean dunes are Late Pleistocene in age (approximately 2 million years old) and correspond with the Bassendean Sand.

We previously identified and studied the Jurien Bay chronosequence, located 200 km north of Perth and receiving approximately 530 mm annual rainfall (Fig. 1, 2A) (Laliberté *et al.*, 2012; Hayes *et al.*, 2014; Laliberté *et al.*, 2014; Turner & Laliberté, 2015; Zemunik *et al.*, 2015; 2016). We now identify three additional chronosequences spanning a strong climate gradient along the coastline. These chronosequences are located near Guilderton, approximately 75 km north of Perth (Fig. 2B), Yalgorup National Park, approximately 100 km south of Perth (Fig. 2C), and at Warren Beach, south of Pemberton and approximately 300 km south of Perth (Fig. 2D). Along each of the three new chronosequences we delineated six to seven chronosequence stages: Holocene (stages 1-3), three Middle Pleistocene (stages 4, 5, or 5a and 5b), and one Early Pleistocene (stage 6). In the three drier chronosequences of the Swan Coastal Plain (Jurien Bay, Guilderton, Yalgorup) these stages correspond to the Quindalup (Holocene), Spearwood (Middle Pleistocene) and Bassendean (Early Pleistocene) dunes (Fig. 2A-C) described by McArthur (2004). On the other hand, the first six stages of the Warren chronosequence are classified as Meerup sand or podzols (Fig. 2D), while the oldest stage is mapped as the Cleave series (Purdie *et al.*, 2004).

Although precise ages of dune formation are not known for any of the chronosequence stages, various lines of evidence support the chronology ranging from the Holocene to the Early Pleistocene (see Turner and Laliberté 2015 for a review). We assume that the broad chronology of dune formation and the relative spatial configuration of dunes are consistent along the entire Swan Coastal Plain (Playford *et al.*, 1976; McArthur, 2004). We also assume that the Swan Coastal Plain chronology is broadly comparable to the main stages of dune formation along the Warren chronosequence (Playford *et al.*, 1976), given that the formation of the main coastal dunes in the region has been driven by the same sea-level high stands during interglacial periods throughout the Pleistocene (Kendrick *et al.*, 1991). Thus, time is constrained only within the limits of our broad estimates about timing of dune formation.

Climate along the chronosequences

Regional variation in precipitation is mapped in Figure 1, while climate data for the four chronosequences are shown in Table 1 and Figure 1. Mean annual rainfall increases from 533 mm at Jurien Bay in the north to 1185 mm at Warren in the south. The dry season, defined as the number of months receiving < 30 mm of rainfall, varies from two months at Warren Beach to seven months at Jurien Bay. Mean annual temperature varies from 15.2°C at Warren in the south to 19.0°C at Jurien Bay in the north. Mean monthly minimum temperatures (January/February) are 10.1°C at Warren and 13.1°C at Jurien Bay, while mean monthly maximum temperatures (July) are 20.3°C at Warren and 25.6°C at Guilderton. The calculated annual potential evapotranspiration ranges from

1133 mm at Warren Beach to 1433 mm at Jurien Bay, reflected in water balances ranging from – 900 mm at Jurien Bay to + 52 mm at Warren.

There is little information on paleoclimate for the four sequences, although it has been argued that the Swan Coastal Plain has been climatically buffered over the lifespan of the sequences (Wyrwoll *et al.*, 2014). In particular, Karri trees (*Eucalyptus diversicolor*) and other moisture sensitive plants in the far southwest of the region did not disappear despite arid conditions further inland.

In Soil Taxonomy, soil moisture and temperature regimes are defined by the control section between 30 and 90 cm in sandy textured soils (Soil Survey Staff, 1999). We do not have soil temperature data for the chronosequences, but can estimate soil temperature regimes from air temperatures at nearby stations. Mean annual air temperature varies between 15.2°C at Pemberton (approximately 18 km from the Warren chronosequence) and 19.0°C at Jurien Bay, and for all sequences the difference between the minimum and maximum mean monthly temperature is > 6°C. The soil temperate regime is therefore Thermic for all four chronosequences. Despite the marked variation in rainfall and potential evapotranspiration along the climate gradient, the four chronosequences all under a xeric moisture regime, because the soil is dry for at least 45 days in summer, wet for at least 45 days in the winter, and moist for more than half the year in total. The latter is marginal at Jurien Bay, where precipitation exceeds evapotranspiration for at least six months of the year. In the eeric moisture regime rainfall is particularly effective for leaching, because it occurs in the winter when potential evapotranspiration is lowest.

Soil sampling

A profile pit was excavated on each of six (Jurien Bay) or seven (all other chronosequences) stages along each chronosequence (Fig. 2). Profile pits were located on the shoulders or upper slopes of dunes, except for the stage-6 profile where dune morphology was indistinct. Pits were at least 1 m deep, and up to 2 m deep on older dunes. Deeper soils were sampled by augering through the pit floor as necessary. However, deep augering was often constrained by dry and incohesive sand that was not retained in the auger, despite the frequent addition of water to the auger hole and the use of a specially designed sand auger (Dormer Soil Samplers, Murwillumbah South, New South Wales, Australia). Soils were described according to Soil Taxonomy (Soil Survey Staff, 1999) and the Australian Soil Classification System (Isbell, 2002) and samples taken from each horizon for bulk density and laboratory analysis. Profile descriptions and analytical data are presented in full in Supplementary Online Material.

To quantify changes in soil nutrients relevant to potential limitation of biological activity, we sampled surface soils (0–10 cm depth) in eighty 10 m × 10 m plots across the four chronosequences (*i.e.* 20 plots per chronosequence). In each chronosequence, we first selected five chronosequence stages (stages 1, 2, 3, 4 and 6) that represented a strong gradient of soil nutrient availability and of the type and strength of nutrient limitation, based on previous work conducted along the Jurien Bay chronosequence (Laliberté *et al.*, 2012; Hayes *et al.*, 2014; Turner & Laliberté, 2015) and on previous soil analyses by McArthur (2004). We excluded the older Spearwood dunes (stages 5a and 5b) from the surface soil sampling as there is relatively little variation in surface soil chemistry between older Spearwood and Bassendean soils (Turner & Laliberté, 2015). For the Jurien Bay chronosequence, we

randomly selected four existing plots used in previous studies (Laliberté *et al.*, 2012; Hayes *et al.*, 2014; Laliberté *et al.*, 2014; Turner & Laliberté, 2015; Zemunik *et al.*, 2015). For the other three chronosequences, we positioned four replicate sampling plots in each of the five chronosequence stages at random positions near the profile pits, ensuring that replicate plots followed the same dune. Replicate plots within each chronosequence stage were >50 m apart. In each plot, we collected four soil samples to 20 cm depth using a 50-mm diameter sand auger. Those four soil samples were bulked and homogenised at the plot level prior to chemical analyses. The homogenised samples were sieved (<2 mm) to remove roots and other large organic debris and then air-dried prior to laboratory analyses.

Soil analysis

Soil analysis for profile pits and surface samples was identical to that described previously (Turner & Laliberté, 2015). Briefly, soil pH was determined in both deionised water and 10 mM $CaCl_2$ in a 1:2 soil to solution ratio using a glass electrode. The concentrations of sand (53 µm–2 mm), silt (2 µm–53 µm), and clay (< 2 µm) sized particles were determined by the pipette method following pretreatment to remove soluble salts and organic matter (Gee & Or, 2002), with further separation of sand fractions by manual dry sieving. Total carbon (C) and N were determined by automated combustion and gas chromatography with thermal conductivity detection using a Thermo Flash 1112 elemental analyser (CE Elantech, Lakewood, NJ). Total P was determined by ignition (550°C, 1 h) and extraction in 1 M H_2SO_4 (16 h, 1:50 soil to solution ratio) (Walker & Adams, 1958). Exchangeable cations were determined by extraction in 0.1 M $BaCl_2$ (2 h, 1:30 soil to solution ratio), with detection by inductively-coupled plasma optical-emission spectrometry (ICP–OES) on an Optima 7300 DV (Perkin-Elmer Ltd, Shelton, CT) (Hendershot *et al.*, 2008). Carbonate was determined by mass loss after addition of 3 M HCl (Loeppert & Suarez, 1996) and organic C was calculated as the difference between total C and $CaCO_3$-C. Bulk density was determined by taking three replicate cores of known volume per horizon using a 7.5 cm diameter stainless steel ring and determining the soil mass after drying at 105°C. Readily-exchangeable phosphate was determined by extraction with anion exchange membranes (resin P) (Turner & Romero, 2009). Total exchangeable bases (TEB) was calculated as the sum of Ca, K, Mg, and Na; effective cation exchange capacity (ECEC) was calculated as the sum of Al, Ca, Fe, K, Mg, Mn, and Na; base saturation was calculated by (TEB ÷ ECEC) × 100.

Leaf area index

Leaf area index (LAI) was estimated in the same plots from which surface soils were collected using a portable plant canopy imager (CI-110, CID Bio-Science, Camas, WA, USA). We took four canopy images per plot, each separated by 7 m. Images were taken with the camera as close to possible to the ground surface to include low-stature vegetation and processed using the built-in software. Leaf area index was calculated using the gap-fraction inversion procedure.

Statistical analysis

Differences in soil properties among chronosequences and chronosequence stages were tested using generalised least squares models using the 'nlme' package in R (Pinheiro & Bates, 2000). Chronosequence and chronosequence stages, and the interaction between these two factors, were

264 treated as fixed factors in the models. Model assumptions were assessed visually and appropriate
265 variance structures were specified in the models if they improved the fit, as determined by
266 likelihood-ratio tests; in general, different variances for each chronosequence and stage
267 combination were used. We calculated 95% confidence intervals from the generalised least square
268 models and used those in graphs; the confidence intervals can be used to visually assess statistically
269 significant differences among means in pairwise comparisons if intervals do not overlap.
270
271 **Results**
272
273 *Vegetation*
274
275 Vegetation varies markedly along the climosequence, from low stature shrubland in the north to
276 relatively tall eucalyptus forest in the south (Fig 3A-D). This change in vegetation structure was
277 reflected in variation in leaf area index, for which maximum values increased from approximately 0.5
278 or less at Jurien Bay in the drier north to 1.5 at Warren Beach in the wetter south (Fig. 3E). Within
279 the sequences, leaf area index generally increased in younger stages and declined in the older
280 stages, although this was less clear for the relatively dry Jurien Bay chronosequence and most
281 pronounced for the wet Warren Beach chronosequence.
282
283 *Pedogenesis along the chronosequences*
284
285 Pedogenesis along all chronosequences followed a similar pattern to that reported previously for the
286 Jurien Bay chronosequence (Turner & Laliberté, 2015). Young soils developed on Holocene dunes
287 were greyish, yellowish, or pale brown, with weakly developed surface horizons enriched with
288 organic matter overlying several meters of unweathered calcareous sand (see Supplementary
289 Material). All young soils contained carbonate and were strongly or very strongly alkaline. Carbonate
290 concentrations in the beach sand and youngest soils were greatest at Jurien (≥ 80% $CaCO_3$), less at
291 Guilderton and Yalgorup (> 40%) and least at Warren (≤5%) (Table 2). This indicates a gradient of
292 declining carbonate concentration in modern parent sand from north to south. Despite this, young
293 soils were of similar strongly alkaline pH throughout the climosequence (Table 2). All soils across the
294 four chronosequences contained > 90% sand (Table 2), predominantly fine, medium, or coarse (0.1 –
295 1.0 mm), with few very fine or very coarse grains (Table S1). Carbonate concentrations declined with
296 pedogenesis in all four chronosequences, and was completely absent from stage 4 profiles (Middle
297 Pleistocene) above the indurated petrocalcic horizons (calcrete). Carbonate depletion occurred
298 earlier in the surface horizons of the two wetter sequences, being evident in stage 2 profiles at
299 Yalgorup and Warren (Table 2, Fig. S1), and was almost completely leached from the stage 3 (old
300 Holocene) dunes at Warren.
301
302 As pedogenesis proceeds and soils begin to acidify the carbonate is progressively leached from the
303 profiles and precipitated at depth, eventually forming an indurated petrocalcic horizon beneath
304 residual yellow sands, characteristic of young Spearwood dunes (i.e. 120,000 years old; stage 4).
305 These soils have brownish yellow subsoil consisting of > 95% residual quartz sand. The yellow colour
306 derives from goethite and the weathering of heavy minerals (Bastian, 1996). Continued pedogenesis
307 leads to progressive leaching of iron oxides, sometimes forming a Bs horizon, and eventually leaving
308 bleached quartz sand profiles several meters deep, characteristic of Bassendean dunes (i.e.

309 approximately 2 million years old; stage 6). These oldest soils have extremely low cation exchange
310 capacity, although base saturation remains high (Table 2).
311
312 The major pedogenic transitions were observed only weakly at Jurien Bay, but were captured clearly
313 in profiles at Guilderton and Yalgorup (Fig. 4). In particular, the old Quindalup dunes (stage 3) at
314 Guilderton exhibited a calcic horizon with weakly cemented secondary carbonates and an incipient
315 undulating petrocalcic horizon (Fig. 4c-e, 4j-k). In contrast, pedogenesis at Warren did not involve
316 the formation of a petrocalcic horizon, presumably due to the lower carbonate content of the parent
317 sand and the greater leaching potential. The old Spearwood dunes at Guilderton, Yalgorup, and
318 Warren all included clear examples of the transition from Spearwood to Bassendean soils, with
319 gradual leaching of iron oxides leading to the development of deep bleached eluvial (E) horizons
320 over yellow sand (Fig. 4f-i, 4l-n). Previous studies at Jurien captured only the initial stage of this
321 process, with a shallow incipient eluvial horizon in the oldest Spearwood dune.
322
323 *Soil Taxonomy*
324
325 Profiles along all four sequences did not generally qualify as Inceptisols because the particle size
326 classes were too coarse for cambic horizons (which require a texture of very fine sand or finer; Table
327 2). As at Jurien Bay, young soils (stages 1–3; Fig. 4a-c) along all four sequences were classified as
328 Psamments (Entisols) because of their coarse sandy texture. Due to the nature of the sand, these
329 young profiles were Quartzipsamments at Warren, but Xeropsamments elsewhere (Table 2). The
330 Xeropsamments were carbonatic, except the youngest soil at Yalgorup, which contained marginally
331 insufficient carbonate in the profile. The oldest Holocene soils at Guilderton and Yalgorup did not
332 qualify as Inceptisols, because the calcic horizons with free secondary carbonates were not within
333 100 cm of the soil surface. In the Australian Soil Classification System (Isbell 2002), the young
334 Holocene soils are predominantly Shelly or Arenic Rudosols, while the old Holocene soils are Calcic
335 or Petrocalcic Tenosols at Guilderton and Yalgorup, and Grey-Orthic Tenosols at Warren.
336
337 Middle and Early Pleistocene soils (stages 4–6; Fig. 4f-i) were Quartzipsamments (Entisols) along all
338 four sequences due to their deep quartz sand profiles lacking diagnostic horizons in the upper part
339 of the profiles. The exceptions were the youngest Spearwood soils at Jurien and Yalgorup, which
340 qualified as Calcic Haploxerepts (Inceptisols) because of the petrocalcic within 150 cm of the soil
341 surface. The stage 4 profile at Guilderton was similar, with contained a petrocalcic horizon below
342 yellow sand, but did not qualify as an Inceptisol because the petrocalcic horizon was > 150 cm below
343 the soil surface. In the Australian Soil Classification system the Middle Pleistocene soils qualify as
344 Grey or Yellow-Orthic Tenosols, with the younger profiles being in the Petrocalcic Great Group, while
345 the older soils with a spodic horizon (stages 5b and 6) qualify as Sesquic or Humosesquic Aeric
346 Podosols.
347
348 Soils from stage 6 (Fig 4i) were morphologically, chemically, and physically similar at each of the four
349 sequences. The designation as Entisols (i.e. young soils) for these 2-million year profiles is an artifact
350 of the Soil Taxonomy system, which does not consider parts of the profile deeper than 200 cm
351 (Turner & Laliberté, 2015). We observed a clear spodic horizon in Bassendean soils only at the
352 Yalgorup chronosequence, although this indurated coffee rock was too deep (>200 cm) for this
353 profile to be placed in the Spodosols. An additional profile at Warren, not on the main

chronosequence but on Bassendean sand, qualified as a Spodosol due to a spodic horizon within 200 cm of the soil surface (see profile classifications in Supplementary Material). Quartz-rich soils often contain insufficient metals to yield a spodic horizon and therefore develop into Quartzipsamments (Fanning & Fanning, 1989), although variation in the presence of a spodic horizon in the Swan Coastal Plain has also been linked to differences in the proximity to the water table (McArthur and Russell 1978). In the absence of spodic horizons, the Bassendean profiles qualify as Grey-Orthic-Tenesols in the Australian Soil Classification System.

Organic carbon, total nitrogen, and total phosphorus

Profile-weighted organic C and N stocks followed a consistent pattern along chronosequences, but were variable across the climosequence (Table 3, Fig. S2, Fig. S3). Stocks of both C and N tended to increase initially to greatest amounts in old Holocene dunes, being as high as 12 kg C m^{-2} / 648.5 g N m^{-2} at Yalgorup (Table 3), and then declined to lower amounts on older dunes. However, organic C was noticeably high in the oldest soil at Guilderton (9.8 kg C m^{-2}) compared to the earlier stages of the sequence.

Total P stocks in the youngest soils (stage 1) were greatest at Jurien (300 g P m-2), lower at Guilderton and Yalgorup (210–240 g P m^{-2}), and lowest at Warren (36 g P m^{-2}), reflecting the carbonate and P content of the parent sand (Table 3, Fig. 5). With the exception of an increasing total P stock in Holocene dunes at Yalgorup, presumably due to high productivity at the old Holocene site (reflected in the high organic C stock), total P declined more or less continuously throughout the chronosequences, reaching extremely low amounts (< 5 g P m^{-2}) on the oldest soils Spearwood and Bassendean soils.

In surface soils (0-10 cm depth) along all four sequences, organic C in surface soils was lowest in the youngest chronosequence stage and then increased to reach maximal values in stage 2 or 3, except for Yalgorup where organic C was also high in the oldest Holocene stage (Fig. 6A). There was a decline in organic C from stage 3 to 4 in three chronosequences (Jurien Bay, Guilderton and Yalgorup), while organic C remained constant from stage 3 to 4 in Warren (Fig. 6A). Total nitrogen followed similar patterns to organic C (Fig. 6B). Total N started at low concentrations in all four chronosequences, then reached maximal values in stage 2 (Jurien Bay) or stage 3 (all other chronosequences). Following this increase, there was a decline in total nitrogen from stage 3 or 4 in all chronosequences (Fig. 6B). In the oldest soils (stage 6), total N reached levels as low as stage 1 for all sequences except Yalgorup (Fig. 6B).

In the three sequences from the Swan Coastal Plain (Jurien Bay, Guilderton, Yalgorup), there were large differences in total P concentrations between the Holocene dunes, which had relatively high total P concentrations, and the older stages, which had extremely low total P concentrations (Fig. 6C). By contrast, total P concentrations in surface soils at Warren were much lower initially (i.e. in stage 1) and increased slightly until stage 4, presumably due to plant uplift and concentration in organic matter at the surface (Laliberté *et al.*, 2012; Turner & Laliberté, 2015), but declined to extremely low concentrations in stage 6 (Fig. 6C).

Along all four chronosequence stages there was a clear increase in the proportion of total P present as organic P during pedogenesis, with organic P reaching almost 100% of surface soil total P in stage 6 for the three wetter sequences (Guilderton, Yalgorup and Warren; Fig. 6D). In general, organic P in surface soils represented a greater proportion of total P as the climate became cooler and wetter (i.e from Jurien Bay to Warren; Fig. 6D).

There were marked increases in surface soil N:P ratio from youngest to oldest stage in all chronosequences (Fig. 6E), eventually reaching high values in the oldest stages (i.e. around 50 or more). The increase was more pronounced in the three drier Swan Coastal Plain chronosequences, whereas N:P increased from stage 1 to 2 at Warren but then did not increase further in older soils (Fig. 6E). Profile-weighted nutrient ratios demonstrated a similar pattern in surface soils (Table 3; Fig. S4). Overall, C:N, C:P, and N:P ratios increased continuously along all four chronosequences, reaching highest values on the oldest soils. For profile-weighted ratios, the greatest values were a C:N ratio of 51.4, C:P ratio of 3764, and N:P ratio of 73.2 in the oldest profile at Guilderton.

Surface soil pH, exchangeable phosphorus, and exchangeable cations

Surface soils in all four chronosequence stages were initially alkaline (pH in 0.01 M $CaCl_2$ > 7) but then gradually acidified during pedogenesis (Fig. 7A). Soil pH in surface soils in stage 1 decreased from the driest to the wettest sequence (i.e. Jurien Bay > Guilderton > Yalgorup > Warren), reflecting the decline in carbonate concentration of the beach sand from Jurien Bay to Warren (Table 2). Similarly, soil pH in the oldest stages was highest at Jurien compared to the other sequences.

Exchangeable phosphorus determined by extraction with anion-exchange resins was highest in the youngest soils of the three drier chronosequences and then declined continuously with pedogenesis, reaching lowest values on the oldest soils (Fig. 7B). In contrast, resin phosphate concentrations at Warren increased initially in Holocene dunes, then declined on Middle and Early Pleistocene dunes (Fig. 7B). Overall, resin P concentrations on the oldest dunes were lower at the driest site (Jurien Bay).

In all four chronosequences, effective cation exchange capacity declined in the oldest soils to reach very low levels (Fig. 7C). However, changes in effective cation exchange capacity during the first three stages differed among chronosequences. In Jurien Bay, and in Guilderton to a lesser degree, there was a general decline in effective cation capacity from the youngest to the oldest soil (Fig. 7C). By contrast, in Yalgorup and Warren, there were increases in effective cation exchange capacity from stages 1 to 3 prior to the decline in the older soils (Fig. 7C). In all stages of all four chronosequences, effective cation exchange capacity was largely dominated by Ca irrespective of soil age, while Mg was the second most important exchangeable cation (Fig. 7C). By contrast, other exchangeable cations (K, Fe, Mn, Na, and Al) were present in very small amounts (Fig. 7C). Base saturation was > 90% in surface soils throughout the four sequences, only being < 100% in Pleistocene soils (Fig. 7D).

Discussion

We define a series of four long-term chronosequences that form a climosequence of chronosequences in southwestern Australia. The system is unique in terms of its Mediterranean

443 climate and its location in a global biodiversity hotspot (Hopper & Gioia, 2004). These four
444 chronosequences allow examination of the influence of climate on patterns of pedogenesis and
445 nutrient status during long-term ecosystem development. Such climate × age systems are
446 exceedingly rare worldwide – the only comparable framework we are aware of is on the Hawaiian
447 Islands, where steep rainfall gradients, well-constrained parent material, and uniform vegetation
448 allow unparalleled control of soil forming factors (Vitousek, 2004).
449
450 Despite relatively large changes in climate, pedogenic change was remarkably consistent along the
451 four chronosequences, with decalcification in Holocene dunes and leaching of iron oxides from
452 Middle Pleistocene dunes, yielding bleached quartz sand profiles several meters deep on Early
453 Pleistocene dunes. These transitions were captured by profiles along the chronosequences,
454 providing evidence that soil variation in the sandplains is a result of in situ soil development.
455 Changes in soil nutrients during ecosystem development were also consistent along the four
456 chronosequences, with increasing N concentrations in young soils, declining concentrations of P and
457 exchangeable cations in old soils, and increasing soil N:P ratios throughout ecosystem development.
458 This pattern of soil nutrients therefore corresponds closely with the Walker and Syers (1976) model
459 of nutrient transformations during pedogenesis. Despite clear effects on vegetation structure (as
460 reflected by changes in LAI), climate effects on soil nutrients appeared marginal, with the only clear
461 variation in soil nutrients with climate manifesting in the nature of the soil P pools. Specifically, the
462 proportion of the soil P present in organic forms was greater, and increased earlier in ecosystem
463 development, in wetter sites, while resin P concentrations were also greater in old Holocene and
464 Middle Pleistocene dunes at the wettest site. These differences suggest that greater plant biomass
465 or productivity maintains P in actively cycling pools, and therefore might buffer against nutrient loss
466 by leaching (Porder & Chadwick, 2009).
467
468 Vitousek and Chadwick (2013b) describe 'soil process domains', in which soil properties change
469 relatively little despite variation in rainfall. These domains occur between 'pedogenic thresholds',
470 where soil properties change rapidly over across a relatively small variation in rainfall. They
471 identified three domains for Andisols about 150,000 years old on Hawaii: (i) a low rainfall domain
472 where evapotranspiration exceeds precipitation and carbonate precipitation dominates; (ii) an
473 intermediate domain where biological uplift of nutrients buffers against loss by leaching, (iii) a high
474 rainfall domain where leaching losses dominate. The intermediate rainfall domain on Hawaii occurs
475 between about 700 and 1700 mm and, based on the results for our Australian climosequence, it
476 appears that the four chronosequences occupy a single process domain: patterns of nutrient
477 availability and pedogenesis are relatively similar across the entire climosequence, and precipitation
478 exceeds potential evapotranspiration only at the most southerly site, and there only marginally (52
479 mm). The lack of variation in patterns of base cations with climate is probably related in part to the
480 sandy nature of the soils, with limited formation of clays or secondary minerals following
481 decalcification. Soil pH and Ca concentrations decline in young soils associated with the depletion of
482 carbonates, exchangeable Al occurs in trace concentrations, and base saturation is therefore always
483 high despite low concentrations of base cations. Indeed, once carbonates are depleted from
484 Holocene soils, and iron oxide coatings leached from the Middle Pleistocene soils, there is essentially
485 no cation exchange capacity other than on organic matter.
486

Vegetation structure varied markedly along the climosequence and within chronosequences. Along the climosequence, vegetation changed from low-stature shrubland in the drier north to relatively tall *Eucalyptus* forest in the wetter south. Given that changes in fertility with increasing soil age appear relatively constant across the four chronosequences, the overall increase in biomass and leaf area index with increasing rainfall is presumably related to water availability. Patterns in vegetation along the chronosequences (i.e. during ecosystem development) was consistent with the concept of retrogression (Wardle *et al.*, 2004), with LAI initially increasing in the early stages of pedogenesis, and then declining on the oldest soils under strong P limitation. This trend was clearest along the wetter chronosequences, where maximum LAI also occurred earlier in ecosystem development, and least clear in the driest chronosequence, where there was no consistent trend in LAI along the chronosequence. Studies so far at Jurien Bay indicate that P availability constrains ecosystem processes and favours plant species with high P-use efficiency on the oldest soils (Laliberté *et al.*, 2012; Hayes *et al.*, 2014), consistent with the concept of retrogression (Peltzer *et al.*, 2010), even if LAI varies little across the chronosequence. For example, the oldest soils are dominated by slow-growing plant species with long-lived leaves that maintain extremely low foliar P concentrations and a high resorption efficiency for P (Hayes *et al.*, 2014).

Ecosystem retrogression therefore appears to be expressed more strongly in the vegetation structure along wetter chronosequences. Along the Australian climosequence, this variation in expression of strong P limitation on the plant community might be influenced by corresponding variation in plant community diversity. Although we have so far not conducted detailed vegetation assessments along all four chronosequences (but see Zemunik *et al.*, 2015; 2016), our field observations indicate declining diversity with increasing rainfall, from the hyperdiverse shrubland at Jurien Bay (Laliberté *et al.*, 2014; Zemunik *et al.*, 2016) to the comparatively low diversity forest at Warren Beach (Hopper & Gioia, 2004). It has been proposed that ecosystem retrogression is less likely to occur in diverse plant communities such as lowland tropical forests because there are more likely to be species that can maintain productivity on low P soils (Kitayama, 2005). For example, the response of the vegetation to changes in nutrient status linked to long-term pedogenesis is relatively clear along the Hawaiian Island chronosequence where forests are dominated by a single species of tree (Vitousek & Farrington, 1997). In contrast, strongly weathered soils at Jurien Bay support a diverse array of species that exhibit high P-use efficiency and can therefore maintain relatively high biomass on extremely infertile soils (Hayes *et al.*, 2014; Lambers *et al.*, 2015; Zemunik *et al.*, 2015). High regional plant diversity might therefore buffer against a decline in productivity related to the long-term decline in P availability during retrogression (Vitousek, 2004).

There are two caveats concerning the chronosequences. First, there is variation in the parent sand along the coastline, with lower carbonate concentrations, and therefore total P concentrations, towards the south. This regional variation in the chemical composition of beach sand is presumably related to differences in offshore productivity (McArthur, 2004), although we do not have information on whether the pattern in modern sand composition also occurred historically. Second, although we find consistent patterns of soil development along the four chronosequences, we have not so far been able to precisely quantify dune ages and therefore rates of soil development. However, the relative dune ages are fairly well constrained, particularly for the Swan Coastal Plain (see also Turner & Laliberté, 2015), giving confidence that the overall patterns are consistent among the four chronosequences. In the Spearwood dunes, Bastian (1996) recognised five stages, although

at least seven sea level high stands are recognised. Aside from the 120,000 year high stand (Marine Isotope Stage 5e) that is relatively easy to identify (and consistent among our chronosequences), a 200,000 year high stand was relatively small and likely to have been over-ridden by the subsequent 120,000 year event. Before that, high stands occurred at approximately 220,000, 240,000, 280,000, 330,000, and 410,000 years, so it is likely that Spearwood stages 4 and 5a in our sequences are separated by at least 100,000 years, but that stages 5a and 5b could be separated by as little as 20,000 years or as much as 190,000 years.

Despite these limitations, we consider that the series of four long-term retrogressive chronosequences across a clear climate gradient provides an important model system for studying long-term soil and ecosystem development, particularly since well-characterised retrogressive sequences are rare worldwide (Peltzer *et al.*, 2010). These four sequences should be particularly valuable as strong natural gradients of soil fertility to explore plant adaptations to declining nutrient availability (e.g. Hayes *et al.*, 2014; Zemunik *et al.*, 2015) and edaphic drivers of plant (Laliberté *et al.*, 2014; Teste *et al.*, 2017) and microbial diversity (Krüger *et al.*, 2015; Albornoz *et al.*, 2016) under contrasting climates, and to examine the independent influence of climate on above and below ground organisms while controlling for variation in soil nutrients.

Acknowledgements

Funding was provided by a Discovery Early Career Researcher Award (DE120100352) and a Discovery Project (DP130100016) from the Australian Research Council, a Research Collaboration Award from The University of Western Australia to EL and BLT, and a NSERC Discovery Grant awarded to EL. The authors thank Dayana Agudo, Pedro Araúz, Aleksandra Bielnicka, and Paola Escobar for laboratory support, and Felipe Albornoz, Hans Lambers, Kenny Png, François Teste, Karl-Heinz Wyrwoll, and Graham Zemunik for assistance in the field. Figure 2 was created using base maps provided by the Department of Agriculture and Food of Western Australia.

References

Albornoz, F.E., Teste, F.P., Lambers, H., Bunce, M., Murray, D.C., White, N.E. & Laliberté, E. 2016. Changes in ectomycorrhizal fungal community composition and declining diversity along a 2-million-year soil chronosequence. *Molecular Ecology*, **25,** 4919-4929.

Bastian, L.V. 1996. Residual soil mineralogy and dune subdivision, Swan Coastal Plain, Western Australia. *Australian Journal of Earth Sciences*, **43,** 31-44.

Chadwick, O.A. & Chorover, J. 2001. The chemistry of pedogenic thresholds. *Geoderma*, **100,** 321-353.

Chadwick, O.A., Gavenda, R.T., Kelly, E.F., Ziegler, K., Olson, C.G., Elliott, W.C. & Hendricks, D.M. 2003. The impact of climate on the biogeochemical functioning of volcanic soils. *Chemical Geology*, **202,** 195-223.

Fanning, D.S. & Fanning, M.C.B. 1989. *Soil Morphology, Genesis and Classification*. John Wiley & Sons, New York.

Feng, J., Turner, B.L., Lü, X., Chen, Z., Wei, K., Tian, J., Wang, C., Luo, W. & Chen, L. 2016. Phosphorus transformations along a large-scale climosequence in arid and semiarid grasslands of northern China. *Global Biogeochemical Cycles*, **30,** 1264-1275.

577 Gee, G.W. & Or, D. 2002. Particle size analysis. In: *Methods of Soil Analysis, Part 4 – Physical*
578 *Methods* (eds. Dane, J.H. & Topp, C.), pp. 255–293. Soil Science Society of America, Madison,
579 WI.
580 Hayes, P., Turner, B.L., Lambers, H. & Laliberté, E. 2014. Foliar nutrient concentrations and
581 resorption efficiency in plants of contrasting nutrient-acquisition strategies along a 2-million-
582 year dune chronosequence. *Journal of Ecology*, **102,** 396-410.
583 Hendershot, W.H., Lalande, H. & Duquette, M. 2008. Chapter 18. Ion exchange and exchangeable
584 cations. In: *Soil Sampling and Methods of Analysis* (eds. Carter, M.R. & Gregorich, E.), pp. 173-
585 178. Canadian Society of Soil Science and CRC Press, Boca Raton, FL.
586 Hopper, S.D. & Gioia, P. 2004. The Southwest Australian Floristic Region: Evolution and conservation
587 of a global hot spot of biodiversity. *Annual Review of Ecology, Evolution, and Systematics*, **35,**
588 623-650.
589 Isbell, R.F. 2002. *The Australian Soil Classification, Revised Edition*. CSIRO Publishing, Collingwood,
590 Victoria, Australia.
591 Jangid, K., Whitman, W.B., Condron, L.M., Turner, B.L. & Williams, M.A. 2013. Soil bacterial
592 community succession during long-term ecosystem development. *Molecular Ecology*, **22,** 3415–
593 3424.
594 Kendrick, G.W., Wyrwoll, K.-H. & Szabo, B.J. 1991. Pliocene-Pleistocene coastal events and history
595 along the western margin of Australia. *Quaternary Science Reviews*, **10,** 419-439.
596 Kitayama, K. 2005. Comment on "Ecosystem properties and forest decline in contrasting long-term
597 chronosequences". *Science*, **308,** 633.
598 Krüger, M., Teste, F.P., Laliberté, E., Lambers, H., Coghlan, M., Zemunik, G. & Bunce, M. 2015. The
599 rise and fall of arbuscular mycorrhizal fungal diversity during ecosystem retrogression.
600 *Molecular Ecology*, **24,** 4912-4930.
601 Laliberté, E., Grace, J.B., Huston, M.A., Lambers, H., Teste, F.P., Turner, B.L. & Wardle, D.A. 2013.
602 How does pedogenesis drive plant diversity? *Trends in Ecology & Evolution*, **28,** 331–340.
603 Laliberté, E., Turner, B.L., Costes, T., Pearse, S.J., Wyrwoll, K.-H., Zemunik, G. & Lambers, H. 2012.
604 Experimental assessment of nutrient limitation along a 2-million-year dune chronosequence in
605 the south-western Australia biodiversity hotspot. *Journal of Ecology*, **100,** 631-642.
606 Laliberté, E., Zemunik, G. & Turner, B.L. 2014. Environmental filtering explains variation in plant
607 diversity along resource gradients. *Science*, **345,** 1602-1605.
608 Lambers, H., Clode, P.L., Hawkins, H.-J., Laliberté, E., Oliveira, R.S., Reddell, P., Shane, M.W., Stitt, M.
609 & Weston, P. 2015. Metabolic Adaptations of the Non-Mycotrophic Proteaceae to Soils With
610 Low Phosphorus Availability. In: *Annual Plant Reviews Volume 48*, pp. 289-335. John Wiley &
611 Sons, Inc.
612 Loeppert, R.H. & Suarez, D.L. 1996. Carbonate and Gypsum. In: *Methods of Soil Analysis, Part 3 –*
613 *Chemical Methods* (ed. Sparks, D.L.E.A.), pp. 437-474. Soil Science Society of America Madison,
614 Wisconsin.
615 McArthur, W.M. 2004. *Reference Soils of South-western Australia*. Department of Agriculture (WA),
616 Perth, Australia.
617 McArthur, W.M. & Bettenay, E. 1974. *Development and Distribution of Soils of the Swan Coastal*
618 *Plain, Western Australia*. Canberra, Australia.
619 Peltzer, D.A., Wardle, D.A., Allison, V.J., Baisden, W.T., Bardgett, R.D., Chadwick, O.A., Condron, L.M.,
620 Parfitt, R.L., Porder, S., Richardson, S.J., Turner, B.L., Vitousek, P.M., Walker, J. & Walker, L.R.
621 2010. Understanding ecosystem retrogression. *Ecological Monographs*, **80,** 509-529.

622 Pinheiro, J.C. & Bates, D.M. 2000. *Mixed-Effects Models in S and S-PLUS*. Springer, New York, USA.
623 Playford, P.E., Cockbain, A.E. & Lowe, G.H. 1976. *Geology of the Perth Basin, Western Australia;*
624 *Bulletin 124 of the Geological Survey of Western Australia*. Geological Survey of Western
625 Australia, Perth, Australia.
626 Porder, S. & Chadwick, O.A. 2009. Climate and soil-age constraints on nutrient uplift and retention
627 by plants. *Ecology*, **90,** 623-636.
628 Purdie, B., Tille, P. & Schoknecht, N. 2004. *Soil-landscape mapping in south-Western Australia: an*
629 *overview of methodology and outputs*. Department of Agriculture and Food, Western Australia,
630 Perth, Australia.
631 Selmants, P.C. & Hart, S.C. 2010. Phosphorus and soil developement: Does the Walker and Syers
632 model apply to semiarid ecosystems? *Ecology*, **91,** 474-484.
633 Soil Survey Staff. 1999. *Soil Taxonomy: A Basic System of Soil Classification for Making and*
634 *Interpreting Soil Surveys*. United States Department of Agriculture–Natural Resources
635 Conservation Service, Lincoln, NE.
636 Teste, F.P., Kardol, P., Turner, B.L., Wardle, D.A., Zemunik, G., Renton, M. & Laliberté, E. 2017. Plant-
637 soil feedback and the maintenance of diversity in Mediterranean-climate shrublands. *Science*,
638 **355,** 173-176.
639 Turner, B.L. & Laliberté, E. 2015. Soil development and nutrient availability along a 2 million-year
640 coastal dune chronosequence under species-rich Mediterranean shrubland in southwestern
641 Australia. *Ecosystems*, **18**, 287-309.
642 Turner, B.L. & Romero, T.E. 2009. Short-term changes in extractable inorganic nutrients during
643 storage of tropical rain forest soils. *Soil Science Society of America Journal*, **73,** 1972-1979.
644 Vitousek, P. & Chadwick, O. 2013a. Pedogenic thresholds and soil process domains in basalt-derived
645 soils. *Ecosystems*, **16,** 1379-1395.
646 Vitousek, P.M. 2004. *Nutrient Cycling and Limitation*. Princeton University Press, Princeton, New
647 Jersey.
648 Vitousek, P.M. & Chadwick, O.A. 2013b. Pedogenic thresholds and soil process domains in basalt-
649 derived soils. *Ecosystems*, **16,** 1379-1395.
650 Vitousek, P.M. & Farrington, H. 1997. Nutrient limitation and soil development: Experimental test of
651 a biogeochemical theory. *Biogeochemistry*, **37,** 63-75.
652 Walker, T.W. & Adams, A.F.R. 1958. Studies on soil organic matter: I. Influence of phosphorus
653 content of parent materials on accumulations of carbon, nitrogen, sulfur, and organic
654 phosphorus in grassland soils. *Soil Science*, **85,** 307-318.
655 Walker, T.W. & Syers, J.K. 1976. The fate of phosphorus during pedogenesis. *Geoderma*, **15,** 1-19.
656 Wardle, D.A., Walker, L.R. & Bardgett, R.D. 2004. Ecosystem properties and forest decline in
657 contrasting long-term chronosequences. *Science*, **305,** 509-513.
658 Williamson, W.M., Wardle, D.A. & Yeates, G.W. 2005. Changes in soil microbial and nematode
659 communities during ecosystem decline across a long-term chronosequence. *Soil Biology and*
660 *Biochemistry*, **37,** 1289-1301.
661 Wyrwoll, K.-H., Turner, B.L. & Findlater, P. 2014. On the origins, geomorphology and soils or the
662 sandplains of south-western Australia. In: *Plant Life on the Sandplains in Southwest Australia, a*
663 *Global Biodiversity Hotspot* (ed. Lambers, H.). University of Western Australia, Crawley,
664 Australia.
665 Zemunik, G., Turner, B.L., Lambers, H. & Laliberté, E. 2015. Diversity of plant nutrient-acquisition
666 strategies increases during long-term ecosystem development. *Nature Plants*, **1**.

667 Zemunik, G., Turner, B.L., Lambers, H. & Laliberté, E. 2016. Increasing plant species diversity and
668 extreme species turnover accompany declining soil fertility along a long-term chronosequence
669 in a biodiversity hotspot. *Journal of Ecology*, **104,** 792-805.

Figure Legends

Figure 1. Map of southwestern Australia, showing isolines for annual rainfall (mm $year^{-1}$) and locations of the four dune chronosequences. Rainfall data are averages from the 1961-1990 period (www.bom.gov.au). The lower panel shows monthly climate data, including precipitation, potential evapotranspiration, and mean temperature for each chronosequence.

Figure 2. Detailed soil classification maps showing the location of the soil sampling sites along the four dune chronosequences: (A) Jurien Bay, (B) Guilderton, (C) Yalgorup and (D) Warren. Mapping of soil systems and subsystems is based on the Western Australian Department of Agriculture soil classification.

Figure 3. (A-D) Changes in vegetation in the oldest chronosequence stage (i.e. stage 6) for each of the four chronosequences, and (E) leaf area index (LAI) along the four dune chronosequences. Leaf area index was not measured on chronosequence stages 5a and 5b. Bar heights represent means (n = 4) and error bars represent 95% confidence intervals from generalised least-square models accounting for different variances among chronosequence stages. Means whose error bars do not overlap can be considered significantly different. Actual values are shown as points. Photo credits: P. Kardol, E. Laliberté, F. Teste, B. Turner and G. Zemunik.

Figure 4. Soil development along the Guilderton chronosequence: (a) young Holocene dune (~100 years, stage 1), (b) medium-aged Holocene dune with incipient A horizon (~1000 years, stage 2), (c) old Holocene dune (6500 years, stage 3), (d) precipitation of pedogenic carbonate forming a calcic horizon in old Holocene dune, (e) surface of a petrocalcic horizon in old Holocene dune, (f) young Middle Pleistocene dune showing decalcified sand coated with iron oxides (120,000 years, stage 4), (g) medium-aged Middle Pleistocene dune with incipient E horizon (~250,000 years, stage 5a), (h) old Middle Pleistocene dune with 1 m deep bleached E horizon (~400,000 years, stage 5b), (i) Early Pleistocene dune showing bleached quartz sand (~2 million years, stage 6). Fine detail in subsoil of five profiles showing key pedogenic stages: (j) a mixture of carbonate and quartz sand-sized grains in young Holocene dune, (k) sand grains cemented by pedogenic carbonate at 150 cm in old Holocene dune, (l) iron oxide coatings on quartz grains in young Middle Pleistocene dune, (m) quartz grains cemented by iron oxide at 250 cm in old Middle Pleistocene dune, (n) clean quartz grains leached of iron oxides in Early Pleistocene dune.

Figure 5. Profile-weighted contents of total P to 100 cm depth along the four dune chronosequences: (A) Jurien Bay, (B) Guilderton, (C) Yalgorup and (D) Warren. Note the differences in the x-axis values among chronosequences.

Figure 6. Changes in (A) organic C, (B) total N, (C) total P, (D) proportion of total P present as organic P, and (E) total N: total P ratio, in surface soils (0-10 cm depth) across the four chronosequences. Bar heights represent means (n = 4) and error bars represent 95% confidence intervals from generalised least-square models accounting for different variances among chronosequence stages. Means whose error bars do not overlap can be considered significantly different. Actual values are shown as points.

715 **Figure 7.** Changes in (A) pH (measured in 0.01 M $CaCl_2$), (B) resin-extractable P, (C) exchangeable
716 cations and effective cation exchange capacity (ECEC), and (D) base saturation, in surface soils (0-10
717 cm depth) across the four chronosequences. In (A), the central horizontal bar in each box shows the
718 median, the box represents the interquartile range, the whiskers show the location of the most
719 extreme data points that are still within a factor of 1.5 of the upper or lower quartiles, and the black
720 points are values that fall outside the whiskers. In B and C, bar heights represent means (n = 4) and
721 error bars represent 95% confidence intervals from generalised least-square models accounting for
722 different variances among chronosequence stages. Means whose error bars do not overlap can be
723 considered significantly different. In B, actual values are shown as points.
724

Table 1. Climate at four long-term chronosequences in southwestern Australia.

Chronosequence [a]	Mean annual temperature (°C) [b]	Monthly mean minimum temperature (°C) [d]	Monthly mean maximum temperature (°C) [e]	Mean annual precipitation (mm)	Potential annual evapotranspiration (mm) [c]	Water balance (mm y^{-1})	Dry season [f]	Dry season rainfall (mm)	Rainfall November to April (mm)
Jurien Bay	19.0 (13.1/24.9)	14.4 (9.3 / 19.5)	24.5 (18.0 / 30.9)	533.2	1433	– 900	October to April	116.2 (21.8% of total)	89.6 (16.8% of total)
Guilderton	18.4 (11.1 / 25.6)	12.3 (6.2 / 18.3)	25.2 (17.1 / 33.3)	653.4	1403	– 750	November to April	97.1 (14.9% of total)	97.1 (14.9% of total)
Yalgorup	17.3 (11.5 / 23.1)	12.3 (7.9 / 16.7)	23.6 (16.1 / 31.0)	943.0	1300	– 357	December to March	65.1 (6.9% of total)	153.7 (16.3% of total)
Warren	15.2 (10.1 / 20.3)	11.1 (7.1 / 15.1)	20.1 (13.7 / 26.5)	1184.9	1133	+ 52	January to February	40.4 (3.4% of total)	247.7 (20.9% of total)

[a] Data from the following Bureau of Meteorology stations: Jurien Bay (009131; 1968–2015), Guilderton Aerodrome (009178; 1996–2015) located 36.6 km from Guilderton, Wokalup (009642; 1951–2015) located 34.7 km from Preston Beach, Pemberton (009592; 1941–2015) located 19 km from Warren Beach.

[b] Mean annual minimum and maximum in parentheses.

[c] Calculated from monthly values from Bureau of Meteorology maps.

[d] Mean monthly minimum and maximum in parentheses. Values are typically between July and August.

[e] Mean monthly minimum and maximum in parentheses. Values are typically between January and February.

[f] Defined as months receiving < 30 mm rainfall, inclusive of stated months.

Table 2. Chronosequence stages, taxonomic classes and features, and profile-weighted soil physical and chemical properties for soils along the Jurien Bay, Guilderton, Yalgorup, and Warren chronosequences, southwestern Australia. ECEC, effective cation exchange capacity.

[a] Data on sand size distribution is presented in Table S1.

[b] Data on Jurien Bay profiles from Turner and Laliberté (2015)

Chronosequence stage	Soil Taxonomy	Carbonate (%)	Sand [a] (%)	Silt (%)	Clay (%)	pH (H_2O)	pH ($CaCl_2$)	ECEC ($cmol_c\ kg^{-1}$)	Base sat. (%)
JURIEN BAY [b]									
1	Carbonatic, thermic, Typic Xeropsamments	82	98.2	1.1	0.7	9.1	8.2	12.93	100.0
2	Carbonatic, thermic, Typic Xeropsamments	66	95.9	2.1	2.0	9.2	8.1	5.52	99.9
3	Siliceous, thermic, Typic Xeropsamments	25	96.9	1.4	1.6	8.9	8.0	5.01	99.4
4	Sandy, siliceous, thermic, Calcic Haploxerepts	0	94.0	2.9	3.1	6.9	6.1	1.94	100.0
5	Thermic, Xeric Quartzipsamments	0	96.7	1.3	2.0	6.8	5.7	0.96	99.9
6	Thermic, Xeric Quartzipsamments	0	97.3	2.3	0.3	5.6	4.4	0.98	97.4
GUILDERTON									
1	Carbonatic, thermic, Typic Xeropsamments	45	98.6	0.1	1.3	9.0	7.5	15.12	100.0
2	Carbonatic, thermic, Typic Xeropsamments	49	97.7	0.7	1.5	9.1	7.7	3.04	100.0
3	Carbonatic, thermic, Typic Xeropsamments	38	92.3	2.3	5.4	8.7	7.3	5.15	100.0
4	Thermic, uncoated, Xeric Quartzipsamments	0	93.5	2.3	4.2	6.0	5.2	0.43	98.6
5a	Thermic, uncoated, Xeric Quartzipsamments	0	95.1	1.5	3.4	5.7	4.8	0.19	87.3
5b	Thermic, uncoated Xeric Quartzipsamments	0	98.5	0.7	0.9	5.5	4.7	0.11	85.6
6	Thermic, uncoated, Xeric Quartzipsamments	0	98.6	0.6	0.8	5.6	3.8	0.68	100.0
YALGORUP									
1	Mixed, thermic, Typic Xeropsamments	37	98.4	0.6	1.0	8.6	6.9	3.08	100.0
2	Carbonatic, thermic, Typic Xeropsamments	48	96.8	0.4	2.8	8.6	7.5	3.98	99.8
3	Carbonatic, thermic, Typic Xeropsamments	42	94.0	1.5	4.5	8.9	7.6	7.21	99.9
4	Sandy, siliceous, thermic, Calcic Haploxerepts	0	97.4	1.2	1.3	6.8	6.3	1.13	98.7
5a	Thermic, uncoated, Xeric Quartzipsamments	0	96.5	2.0	1.5	6.2	5.0	0.44	91.5
5b	Thermic, uncoated, Xeric Quartzipsamments	0	98.0	1.1	0.9	5.9	4.2	0.16	84.0
6	Thermic, uncoated, Xeric Quartzipsamments	0	97.1	2.4	0.5	5.9	4.1	0.30	94.3
WARREN									
1	Thermic, uncoated, Xeric Quartzipsamments	4.2	99.1	0.5	0.4	9.2	8.1	3.79	99.9
2	Thermic, uncoated, Xeric Quartzipsamments	1.5	99.1	0.3	0.6	9.0	8.1	2.36	100.0
3	Thermic, uncoated, Xeric Quartzipsamments	0.2	97.8	1.7	0.5	6.2	5.3	1.05	93.5
4	Thermic, uncoated, Xeric Quartzipsamments	0	98.9	0.6	0.5	5.8	4.9	0.35	80.1
5a	Thermic, uncoated, Xeric Quartzipsamments	0	98.9	0.6	0.6	5.9	4.7	0.51	94.4
5b	Thermic, uncoated, Xeric Quartzipsamments	0	98.9	0.6	0.5	5.3	4.2	0.68	97.2
6	Thermic, uncoated, Xeric Quartzipsamments	0	98.8	0.7	0.5	5.3	4.0	0.27	94.9

Table 3. Profile weighted nutrient concentrations for the upper 100 cm of soil in profile pits along the Jurien Bay, Guilderton, Yalgorup, and Warren chronosequences, southwestern Australia. Data for the Jurien Bay chronosequence are from Turner & Laliberté (2015).

Chronosequence stage	Organic C ($g\ m^{-2}$)	Total N ($g\ m^{-2}$)	Total P ($g\ m^{-2}$)	C:N	C:P	N:P
JURIEN BAY						
1	8900	495.5	384.3	18.0	23.2	1.3
2	14678	763.3	346.4	19.2	42.4	2.2
3	17720	362.2	194.8	48.9	90.9	1.9
4	3864	166.5	28.8	23.2	134.4	5.8
5	2917	119.2	12.7	24.5	228.9	9.4
6	4063	117.8	6.4	34.5	639.2	18.5
GUILDERTON						
1	2165	223.3	240.1	9.7	9.0	0.9
2	4284	371.4	136.3	11.5	31.4	2.7
3	7282	537.7	198.5	13.5	36.7	2.7
4	1500	110.8	14.5	13.5	103.3	7.1
5a	1924	102.0	10.9	18.9	177.2	9.4
5b	1772	54.3	3.1	32.6	565.6	17.3
6	9801	190.7	2.6	51.4	3764.4	73.2
YALGORUP						
1	3324	224.5	210.0	14.8	15.8	1.1
2	6030	503.0	219.5	12.0	27.5	2.3
3	12162	648.6	277.7	18.7	43.8	2.3
4	4922	200.8	31.4	24.5	156.9	6.4
5a	3336	117.5	6.6	28.4	508.7	17.9
5b	6153	151.8	4.3	40.5	1434.8	35.4
6	5430	181.0	5.6	30.0	976.7	32.6
WARREN						
1	188	47.9	35.6	3.9	5.3	1.3
2	2055	145.7	23.0	14.1	89.2	6.3
3	3337	239.5	18.4	13.9	181.4	13.0
4	1925	99.4	11.4	19.4	169.5	8.8
5a	2820	148.3	4.4	19.0	636.3	33.5
5b	3932	140.2	4.5	28.0	869.0	31.0
6	2675	74.1	2.3	36.1	1141.1	31.6

Figure 1

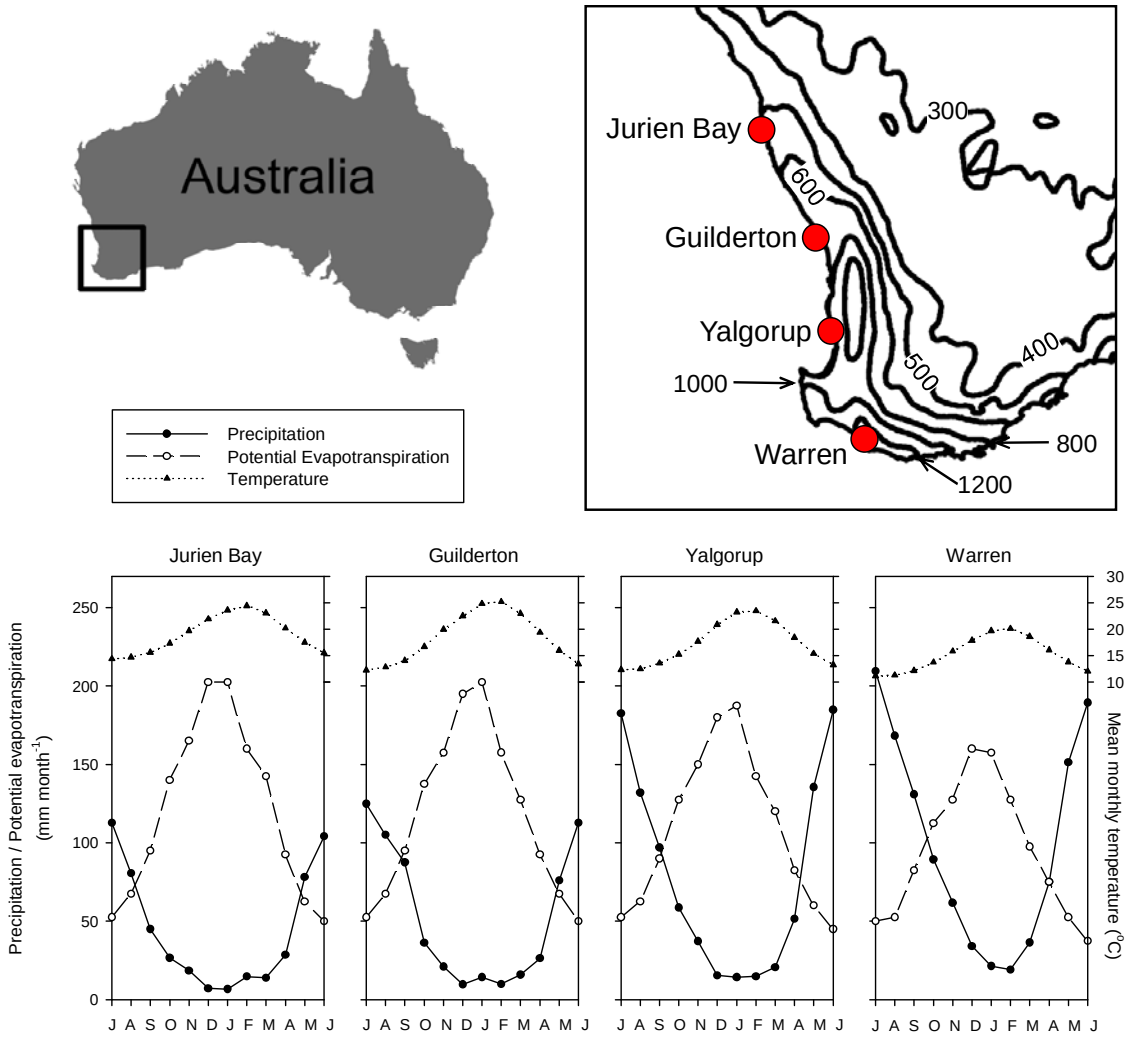

Figure 2

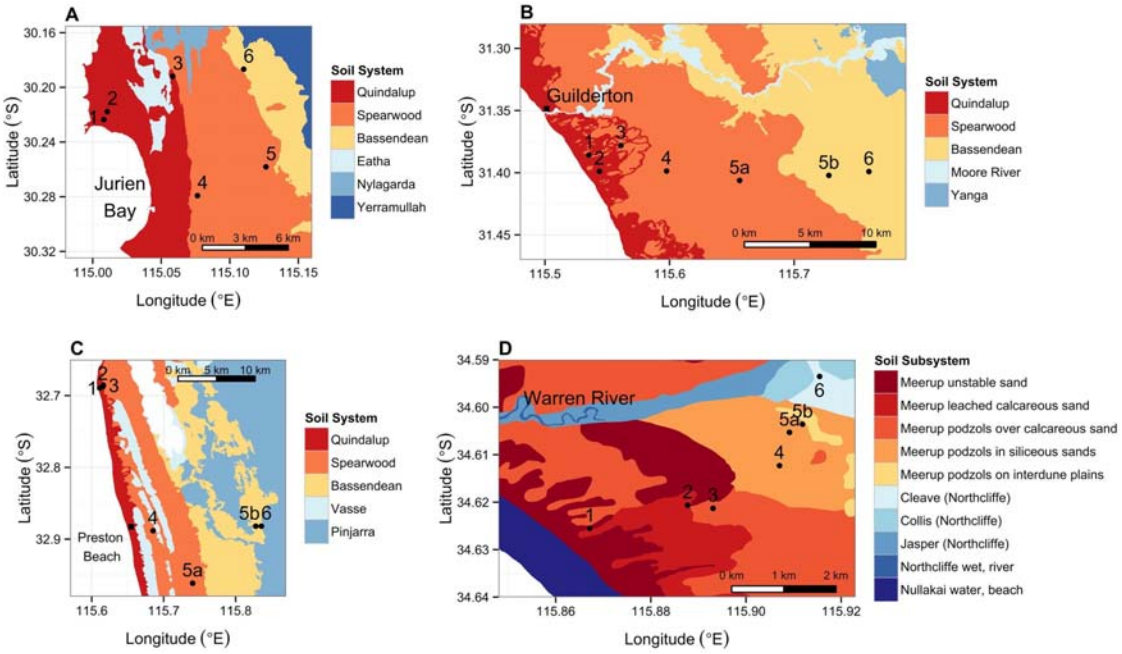

Figure 3

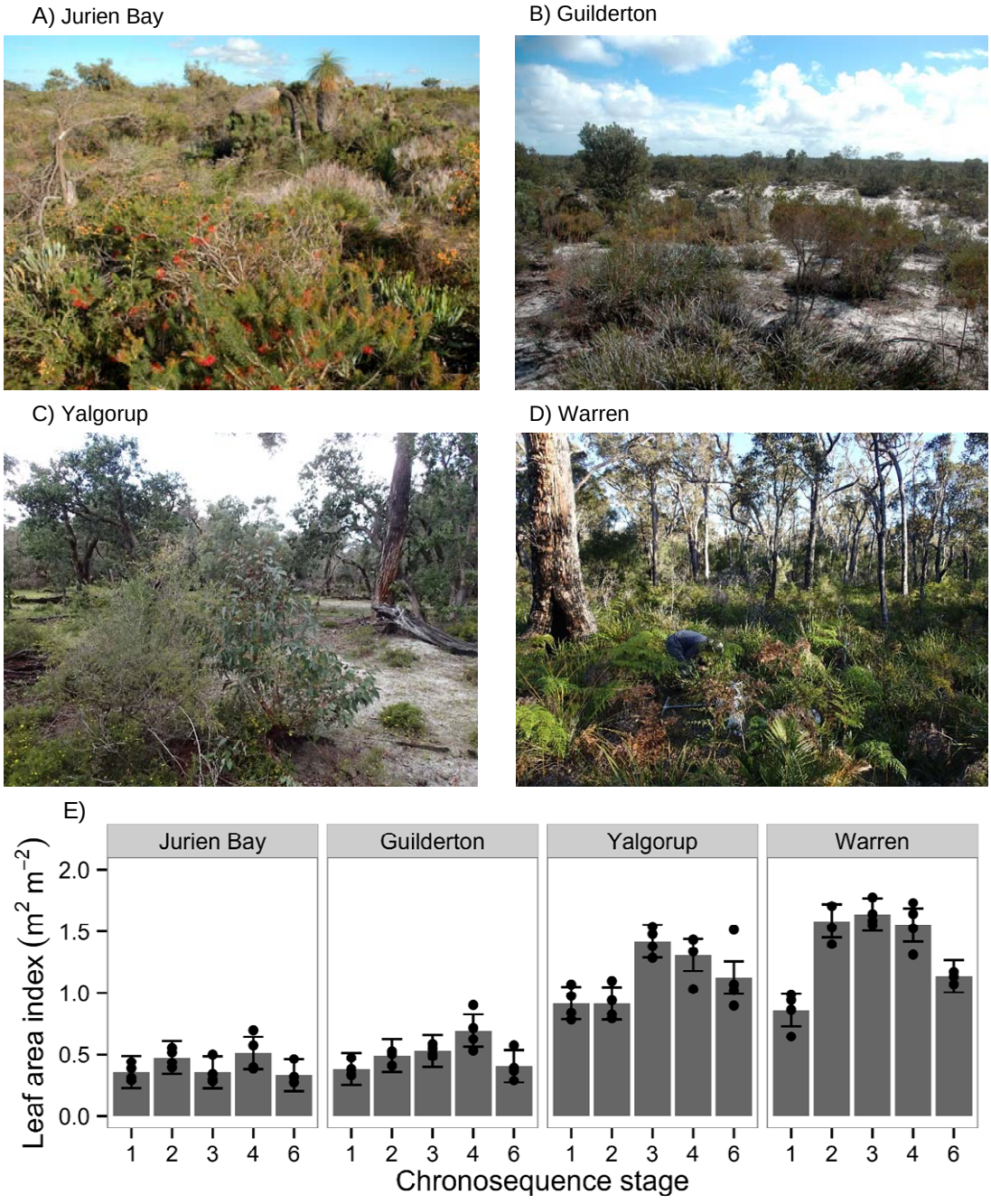

Figure 4

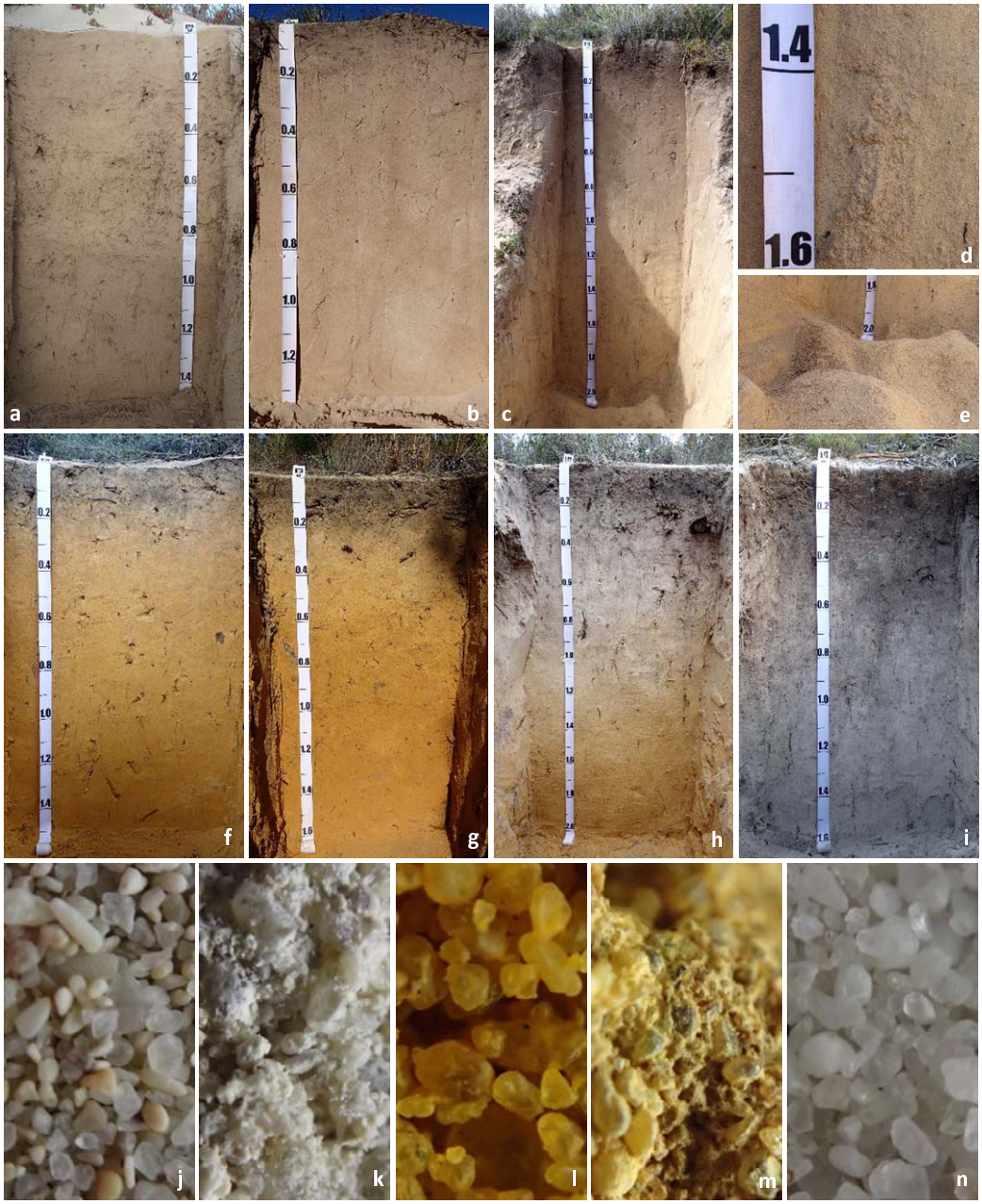

Figure 5

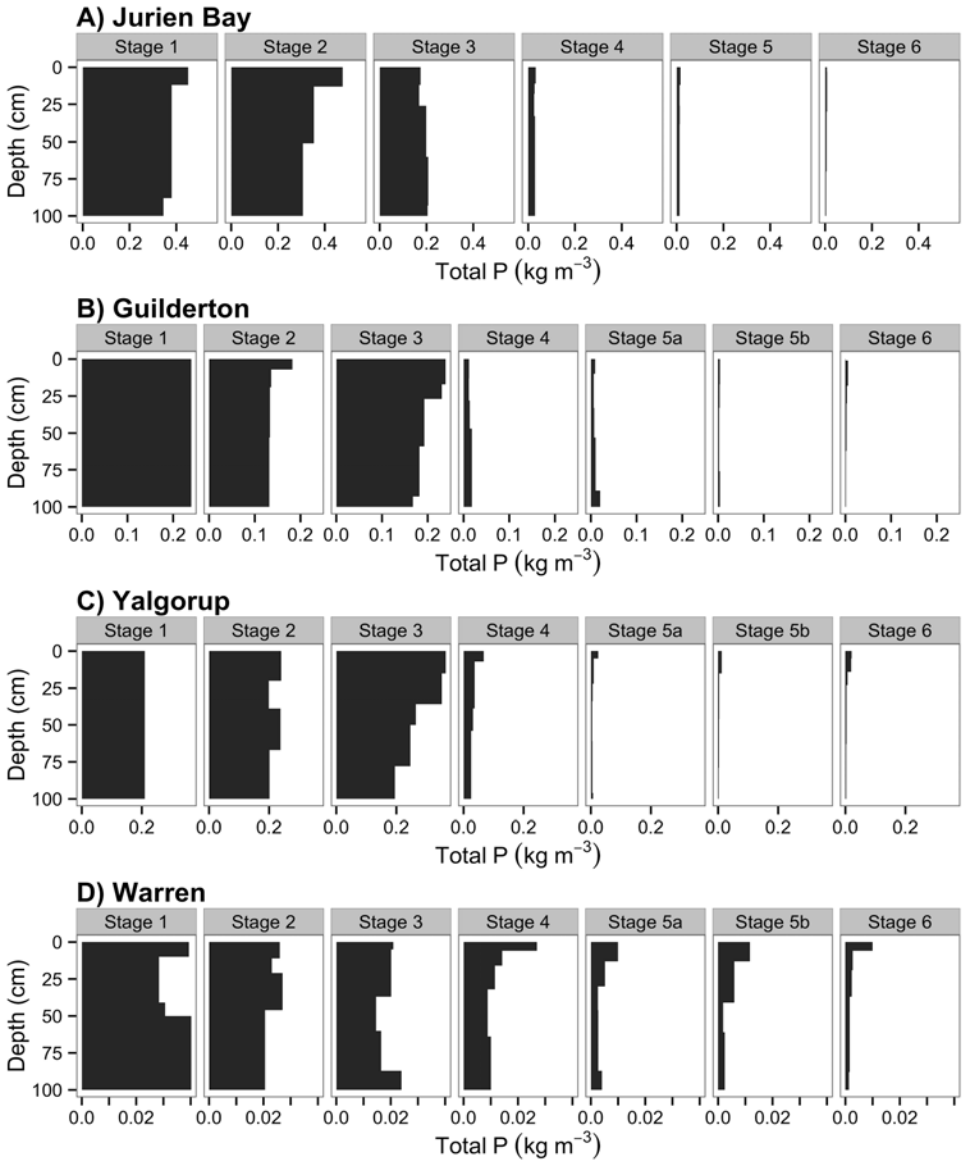

Figure 6

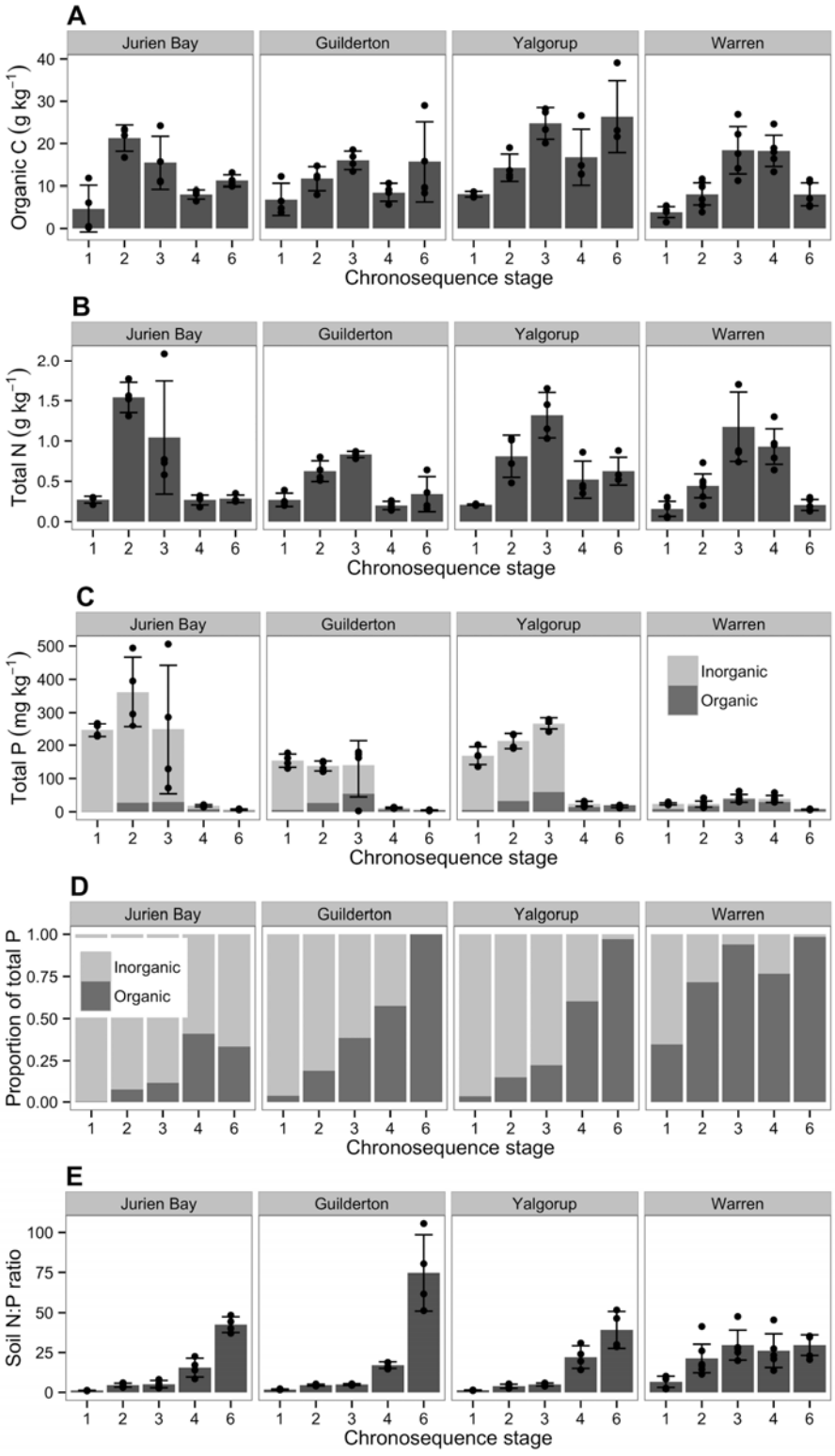

Figure 7